Distinct mobility patterns of BRCA2 molecules at DNA damage sites

Maarten W. Paul[1,✉], Jesse Aaron[2], Eric Wait[2,3], Romano M. van Genderen[1], Ihor Smal[1,4], Teng-Leong Chew[2], Roland Kanaar[1], and Claire Wyman[1,5]

[1]Department of Molecular Genetics, Oncode Institute, Erasmus MC Cancer Institute, Erasmus University Medical Center, Rotterdam, Netherlands
[2]Advanced Imaging Center, HHMI Janelia, Ashburn VA, United States
[3]Elephas Biosciences, Madison WI, United States
[4]Theme Biomedical Sciences, Erasmus University Medical Center, Rotterdam, Netherlands
[5]Department of Radiation Oncology, Erasmus MC Cancer Institute, Erasmus University Medical Center, Rotterdam, Netherlands

BRCA2 is an essential tumor suppressor protein involved in promoting faithful repair of DNA lesions. The activity of BRCA2 needs to be tuned precisely to be active when and where it is needed. Here, we quantified the spatio-temporal dynamics of BRCA2 in living cells using aberration-corrected multifocal microscopy (acMFM). Using multicolor imaging to identify DNA damage sites, we were able to quantify its dynamic motion patterns in the nucleus and at DNA damage sites. While a large fraction of BRCA2 molecules localized near DNA damage sites appear immobile, an additional fraction of molecules exhibit restricted motion, providing a potential mechanism to retain an increased number of molecules at DNA lesions. Super-resolution microscopy revealed inhomogeneous localization of BRCA2 relative to other DNA repair factors at sites of DNA damage. This suggests the presence of multiple subcompartments at the chromatin surrounding the DNA lesion, which may play an important role in the contribution of BRCA2 to the regulation of the repair process.

DNA repair | BRCA2 | Nuclear organization | Single-molecule tracking | Multi-color multi-plane 3D microscopy

Correspondence: ***m.w.paul@erasmusmc.nl***

Significance statement

During homology-mediated DNA double-strand break repair, BRCA2 is required to be present at DNA damage sites to mediate repair. One of its functions is to organize RAD51 in its central role of homology recognition. Using multifocal 3D single-molecule tracking, we show that BRCA2 exhibits specific restricted motion at marked DNA damage sites, while super-resolution microscopy reveals a clustered localization pattern for BRCA2. This work contributes to our understanding of how nuclear proteins organize in the nucleus to control essential processes. The observed dynamics and nanoscale organization of BRCA2 helps to understand how BRCA2 localizes to DNA lesions to exert its function when and only when it is needed.

Introduction

The activity of proteins needs to be controlled spatially and temporally. This is especially true for proteins that maintain the integrity of the genome through DNA repair reactions. Those proteins must act at the right place and time to repair DNA damage. They need to cooperate or compete with many other proteins at the same genomic location, such as proteins involved in replication and transcription. Critical parameters that define the activity of these proteins in cells are their concentration and their diffusion rate. Simultaneously both transient, non-specific and specific interactions determine their spatial organization. These specific and nonspecific interactions can be with other proteins but also with other biomolecules such as DNA and RNA.

BRCA2 is an essential DNA repair protein that is present at a low concentration in the cell nucleus. It is found in a complex with several other DNA repair proteins, such as PALB2 and RAD51, that are all required at sites of DNA damage lesions repaired through homologous recombination (1). The central function of BRCA2 is to exchange the single-strand DNA binding protein complex, RPA, with RAD51 on the resected DNA ends of DNA double-strand breaks (DSB). Additionally, resolution of stalled replication forks and of interstrand crosslinks by homologous recombination require the localized activity of BRCA2 at damage sites (2, 3). As an important tumor suppressor, BRCA2 is an extensively studied protein, where BRCA2 mutations are associated with hereditary breast and ovarian cancer (4). Nonetheless the biophysical properties of BRCA2 that drive its function in cells are not fully understood. Here, our objective is to define the dynamic behavior of BRCA2 around DNA lesions to understand the critical parameters that are required for BRCA2 to act properly.

DNA-associated proteins can exhibit different modes of diffusion contributing to their different functions (5, 6). For example, recently it has been reported that the transcriptional regulator CTCF maintains transient binding zones within the cell nucleus which could be a mechanism to improve its target search efficiency in the nuclear volume (7). Although many nuclear proteins, such as transcription factors, are involved in direct and specific interactions with DNA (sequence motifs, specific structures), it appears that BRCA2 does not depend on this type of interaction for its immobilization at damage sites, but rather on (transient) protein-protein interactions (8). The immobilization and accumulation of BRCA2 is essential for its function, but what interactions are relevant for this behavior and how this correlates with its function is largely unknown. Several reports indicate a crucial interaction between BRCA2 and PALB2, and indeed BRCA2 accumulation at damage sites depends on the interaction with PALB2 (9). Recent data suggests that PALB2 chromatin interaction depends on chromatin associated proteins (10, 11), hence those chromatin interactions could also contribute to the diffusive patterns that have been observed for BRCA2 (8, 12).

BRCA2 accumulates at sites of DNA damage, into so-called foci, like several other homologous recombination repair proteins. It is not yet fully understood how the redistribution occurs and how BRCA2 proteins organize themselves at sites of damage. In this study, we applied 3D single-molecule multiplane imaging to define the quantitative behavior of endogenous BRCA2 at fluorescently marked DNA damage sites. This revealed that at DNA damage sites immobilization of BRCA2 is increased, but also that those molecules that diffuse near DNA lesions do so with increased confined mobility. Quantification of the amount of BRCA2 molecules in the nucleus and at damage sites indicated that only tens of BRCA2 molecules are present per focus, while super-resolution microscopy confirmed the localization of BRCA2 in nanoscale clusters within foci.

Results

In previous studies we have shown, by various imaging techniques, that BRCA2 appears more immobile after induction of DNA damage (8, 12). Those studies, however, did not investigate the spatial distribution of immobilized BRCA2 upon induction of DNA damage. BRCA2 is involved in the repair of different types of lesions that also involve RAD51 mediated homology recognition and DNA strand exchange. One type of lesion requiring BRCA2 for repair is the interstrand-crosslink, which can be induced by chemical reagents such as mitomycin C. The formation of BRCA2 foci after mitomycin C treatment is correlated with the observation that BRCA2 becomes more immobile and suggests that induction of DNA damage causes a redistribution of BRCA2 to DNA damage sites (12). In this study, we use a previously generated mouse embryonic stem (ES) cell line in which endogenous BRCA2 is homozygously tagged with a HaloTag by knock-in mediated by CRISPR / Cas9. This enables direct, real-time visualization of individual BRCA2 molecules in living cells. Here, we used this cell line (as described by Paul et al., 2021) to investigate the mobility of BRCA2 at damage sites by applying spot-FRAP at BRCA2-HaloTag mitomycin C-induced DNA repair foci. These experiments show a large immobile fraction of BRCA2 at sites of damage, with only 50% fluorescence recovery of the prebleached signal during 50 seconds of data acquisition (Figure 1A). This large immobile fraction is not observed for BRCA2 in the nucleoplasm outside the foci, although the low concentration of BRCA2 in the cell nucleus makes these measurements challenging. Taken together, our FRAP experiment suggests that upon induction of DNA damage, part of the BRCA2 molecules is confined to local DNA damage sites.

3D single-molecule tracking reveals the immobilization of BRCA2 at individual DNA repair foci

Although FRAP is a powerful technique for studying the dynamic exchange of proteins in cells, its application is limited to studying the underlying diffusive behavior of proteins at the single-molecule level, which can be investigated with single-molecule tracking (13). To investigate changes in BRCA2 at DNA damage sites specifically, single-plane particle tracking has limitations. One of the limitations of 2D single-molecule tracking is the restrictions of the imaging volume, where molecules can move in and out of the focal plane. While the axial excitation thickness for HiLo illumination acquisition is in the range of 1-2 µm, the cell nucleus is about 5 µm thick. Furthermore, the DNA repair foci, in which BRCA2 dynamics needs to be quantitated, are distributed across the entire nuclear volume and, therefore, it is not possible to capture all foci in one focal plane, and hence some of the foci will be out of focus.

Furthermore, both cell nuclei and DNA repair foci are dynamic in their composition and spatial location within the nucleus (14, 15), therefore the regions from which data should be recorded are moving during image acquisition. To address these challenges, we have applied 3D single-molecule tracking of the whole nucleus using a multicolor aberration-corrected multifocus microscope (acMFM) (16) (Figure 1B). Using this microscope, nine focal planes are projected (approximately 400 nm spacing) on a single camera chip. This allows for rapid instantaneous 3D imaging at 9 planes. To identify the sites of DNA damage, EGFP-tr53bp1 was introduced in the cells as a marker of DNA breaks. This construct expressing a fragment of the 53bp1 protein (a.a. 1221-1709) is a good marker for DNA breaks and was validated previously to not interfere with the repair process (17–19). Immunofluorescence experiments confirmed the proper localization of the tr53bp1 protein in our cells, overlapping with the signal of endogenous 53bp1. Upon treatment with DNA crosslinking agent mitomycin C foci of tr53bp1 can be observed that co-localize with BRCA2 accumu-

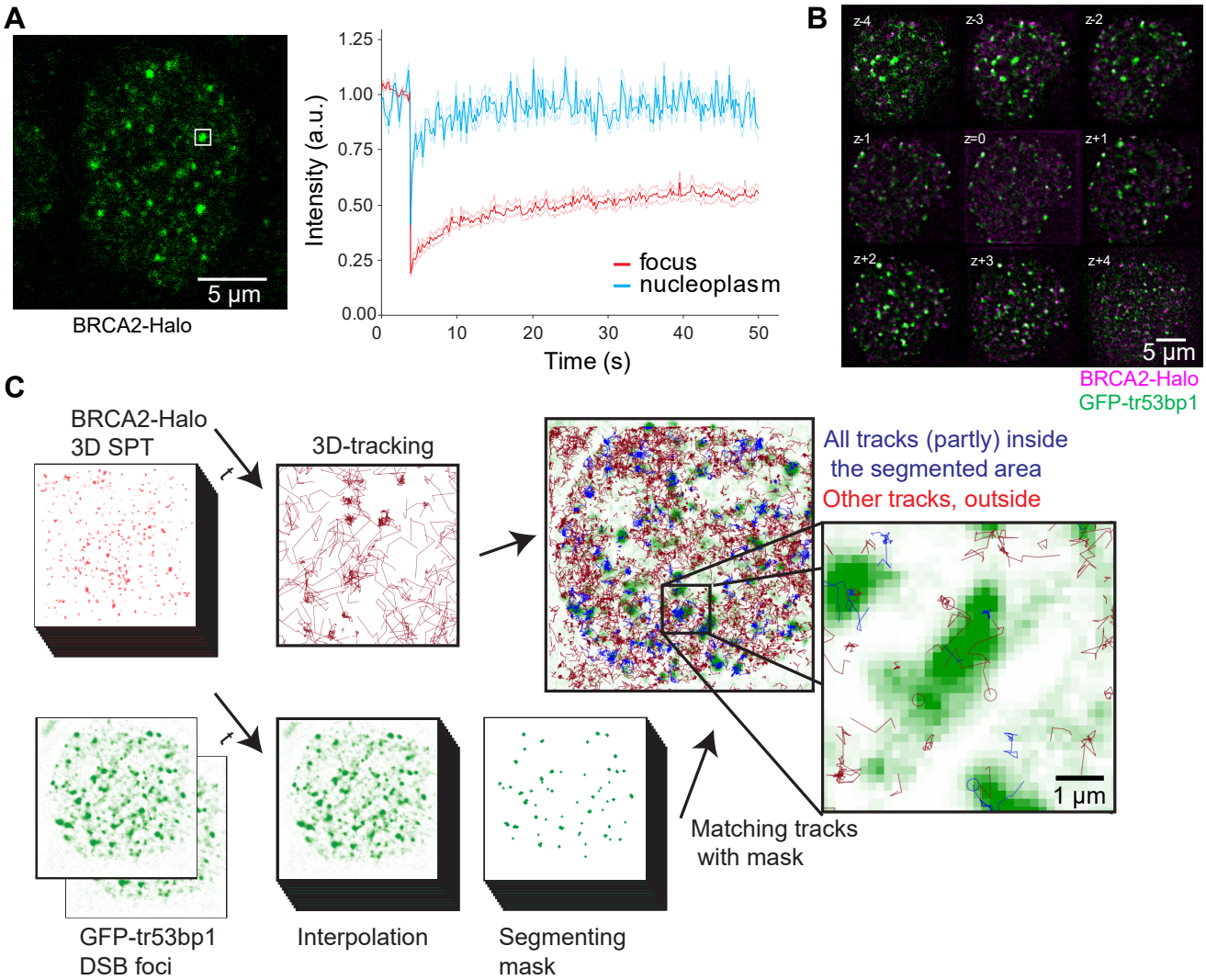

Figure 1. Analysis of the mobility of BRCA2 at sites of DNA damage. A Spot-FRAP of BRCA2-HaloTag cells treated with mitomycin C by photobleaching a focus or region in the cytoplasm (3 independent replicates, focus n=40, nucleoplasm n=20 cells, shading around the curve indicates SEM) **B** Example of a single multi-focal plane image showing 9 z-plane projections spaced 420 nm apart; the signal of BRCA2-Halo (magenta) and EGFP-tr53bp1 (green) is shown. **C** Approach for analysis of molecule tracks in and outside the foci, by matching the localized molecules to the binary mask of the damage sites defined by the 53bp1 signal. See Figure 1 – supplementary movie 1-3 for movies of this data.

lations (Figure S1). By applying single-molecule tracking and simultaneously following the foci distribution in the cells we directly correlate the diffusive behavior of BRCA2 with regions of DNA damage (Figure 1C). The developed image analysis routine allows us to identify whenever a single BRCA2 molecule is within a region of damage during image acquisition.

Using the described approach, we investigated the motion patterns of BRCA2 specifically

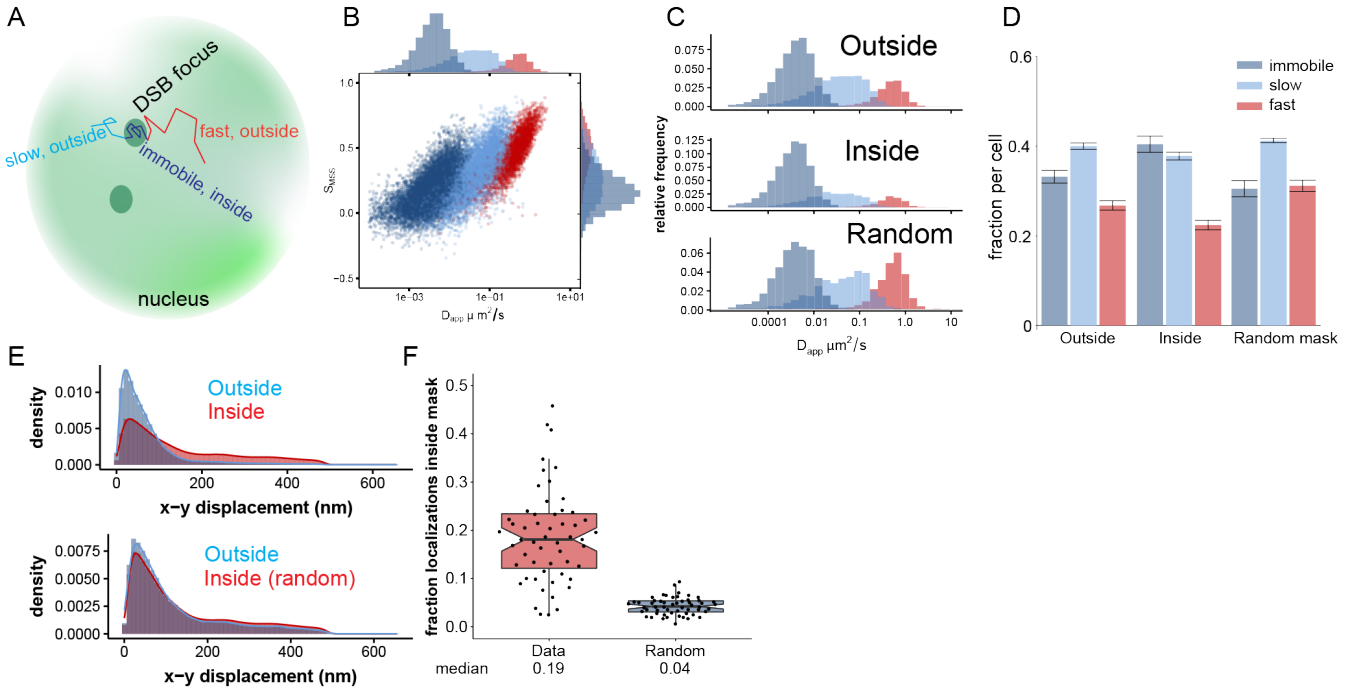

Figure 2. In depth analysis of mobility in and outside the foci. A All track segments (tracklets) in the data set are annotated as being in or outside the DSB foci and having a fast, slow, or immobile state. **B, C** Segmentation of tracks into tracklets with 3 defined diffusive states of BRCA2 (immobile, slow and fast), shown for tracklets outside the focus mask, inside and inside a randomized mask as described in material and methods. The data consists of 4 independent experiments of 55 cells in total. The histogram displays the overall distribution of all cells imaged. **D** Quantification of the distribution of tracklets outside, inside and inside random mask. The indicated fraction is estimated from the mean fraction per cell. **E** Distribution of mean x-y displacements for track segments outside versus inside the DSB foci mask. Plot below shows the distribution but for a random mask. **F** Fraction of localizations in and outside the defined mask for the data compared to the random mask.

at sites of DNA damage. We defined molecules to be inside of the focus if they reside at least one frame (50 ms) inside the tr53BP1 defined focus volume (Figure 1C, Figure 2A). For this analysis we have defined a binary mask of the 53bp1 signal during the acquisition of the single-molecule tracking movie. This definition allows for comparison of tracked molecules that are inside or in close proximity of the foci, with tracks outside the foci, without introducing edge effects caused by using a binary mask: immobile molecules will have a higher chance of staying within the mask for a longer time and hence will be identified more frequently if we would do the analysis where the entire track needs to be inside the mask.

Since we have previously observed that BRCA2 molecules can frequently switch between different diffusive states we applied a recently developed deep learning approach method to our single-molecule tracking data to segment tracks into tracklets (20). With this method we have defined three different diffusive states for BRCA2: fast, slow and immobile. The analysis of the slope of the moment scaling spectrum (Smss), a measure for the diffusivity of molecules, showed that both the immobile and slow molecules exhibit a confined motion pattern (Figure 2B). The analysis of mean-square displacement confirms that there is a

clear enrichment in the amount of BRCA2 tracklets (41% inside vs 32% outside) in the immobile state at the identified DNA damage sites while the diffusion rates of the different fractions are not affected (Figure 2C,D). We observe that the diffusion rate of fast diffusing molecules is 0.55 $\mu m^2/s$, whereas slow diffusing and immobile BRCA2 molecules have, respectively, an apparent diffusion constant of 0.06 $\mu m^2/s$ and 0.005 $\mu m^2/s$, comparable to previous studies (8, 12, 20). To validate the observed differences in the fraction of immobile molecules between the in- and outside-of-the-DNA repair foci, we also analyzed the data after randomly redistributing the segmented foci objects along the x- and y-axes of the image plane (see Methods for details). Compared to the original data, the randomized data shows no increase in immobile molecules compared to outside (Figure 2C-E). Furthermore, we observe 2.7 times more localizations in real foci compared to randomly defined foci, confirming the observation that BRCA2 accumulates at tr53bp1 foci (Figure 2F).

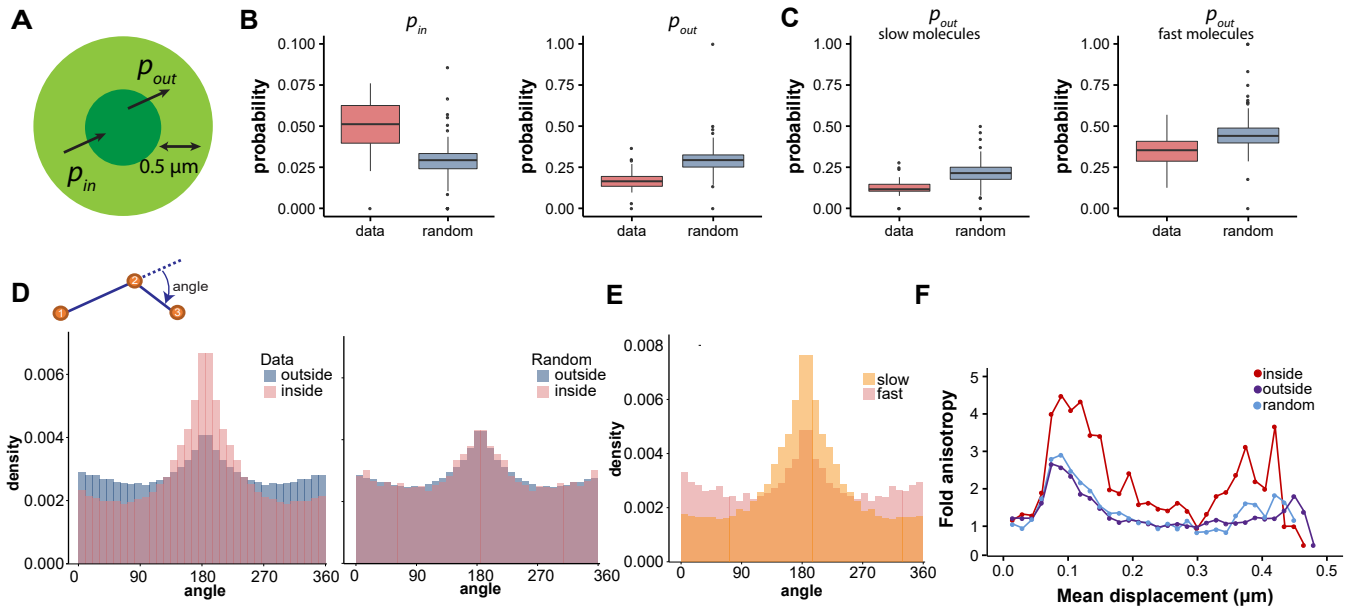

Figure 3. Analysis of in-out transitions and confined motion of BRCA2 at DNA damage sites. A, B In-out transition analysis. For diffusing molecules (excluding immobile tracks) that are within 0.5 µm of the mask the probability that they move into the mask at the subsequent track step is estimated and compared to the random mask (p_{in}), or the probability that a molecule moves out of the mask (p_{out}). In **C** p_{out} is shown for slow- or fast-diffusion molecules. The box plots show the distribution of probability determined per imaged cell. **D** By determining the angle between subsequent localized molecules, anisotropy in the mobility of molecules can determined. Displacements of immobile molecules are excluded from the analysis. The determined distribution of angles for BRCA2 is plotted for all molecules outside and inside the damage site and compared to a randomized mask. **E** The distribution of fast and slow moving molecules **F** The distribution of the fold anisotropy (ratio between backward angle (180 +/- 15 degrees) versus forward angle (0 +/- 15 degrees) plotted against mean displacement of the track.

Diffusive BRCA2 molecules are confined at DNA repair foci

Next, we used the 3D tracking data to investigate the exchange of BRCA2 from the foci with the rest of the nucleoplasm (Figure 3A-C). We compared the probability that a molecule outside the mask, but within 0.5 µm from the focus, will move into the focus in the next step of the track. This showed that the observed fraction of molecules that move

from outside to inside in every image frame is significantly higher compared to that with a random mask (5% vs 2.5%) (Figure 3B). Subsequently, we determined the probability that a molecule would move from inside the mask to outside and observed that in the experimental data, the probability is lower compared to the randomized mask (18% vs 28%) (Figure 3B). When the data are divided into slow and fast tracklets, we do observe that this reduced probability is contributed by the slow molecules having a higher chance of staying in the masked area (Figure 3C).

Diffusive BRCA2 molecules exhibit specific confined motion patterns in DNA repair foci

One of the explanations for the increased concentration of BRCA2 molecules at the damage sites and its propensity to remain in these accumulations could be that BRCA2 molecules exhibit confined motion. One approach to determine the anomalous diffusion of proteins in cells is to look at the anisotropic movement of the tracked molecules. Molecules that exhibit normal diffusion will move in a random direction independent of its previous position, but when motion is confined, molecules will move more frequently in a certain direction with respect to the previous location (5, 7). To only look at diffusive protein molecules, tracklets that are assigned by our state segmentation method as immobile were excluded from the analysis. In fact, mobile BRCA2 molecules appear to have an anisotropic motion pattern, and anisotropic mobility appears to be more enhanced at DNA repair foci (Figure 3D). This appears to be the case mainly for slow diffusion molecules, as the faster diffusing molecules show this behavior to a lesser extent (Figure 3E). We quantified the fold increase in the backward angle (180 +/- 15 degrees) versus forward angle (0 +/- 15 degrees) compared to the average displacement of the tracked molecule at that time (Figure 3F). We can observe a peak between 80 and 150 nm of the average displacement, which suggests that especially molecules that have shorter displacement show confined motion.

BRCA2 localizes in multiple clusters of several BRCA2-molecules at DNA repair foci

To further understand the organization of BRCA2 in the foci, we have applied dSTORM imaging of BRCA2-Halo to visualize the spatial arrangement of BRCA2 under similar experimental conditions at 53bp1 foci after mitomycin C treatment. Previous experiments in human cells using anti-BRCA2 antibodies showed the presence of multiple BRCA2 clusters per focus (21). By using direct HaloTag labeling of BRCA2-Halo with Alexa647-HaloTag ligand we can accurately localize BRCA2 in foci by single-molecule localization microscopy. We used 53bp1 foci to identify regions of interest to visualize BRCA2 localization. Comparison of the localization of 53bp1 and BRCA2 in the foci indicates that BRCA2 is frequently excluded from regions that are dense in 53bp1 signal (Figure 4A). Within the 53bp1 foci we quantified BRCA2 to localize in several small clusters of about 50 nm in size (Figure 4A-C). Furthermore, we quantified the distance between BRCA2 clusters (Figure 4D). This analysis shows that most BRCA2 clusters are 200 nm spaced apart with respect to their center-of-masses.

Subsequently we aimed to estimate the concentration of BRCA2 in mouse ES cell nuclei. For this purpose, we imaged live BRCA2-HaloTag cells by confocal microscopy, while titrating known concentrations of JF646-labeled GST-HaloTag protein in the cell culture medium. This allowed us to determine the correlation between voxel intensity and HaloTag protein concentration (Figure 4E, Figure S2). Although we did not estimate the actual excitation confocal volume of a voxel, we were able to determine the local concentration of BRCA2-Halo per pixel. With the assumption that the nuclei and foci are larger than the confocal volume we can use the integrated intensity of the objects to estimate

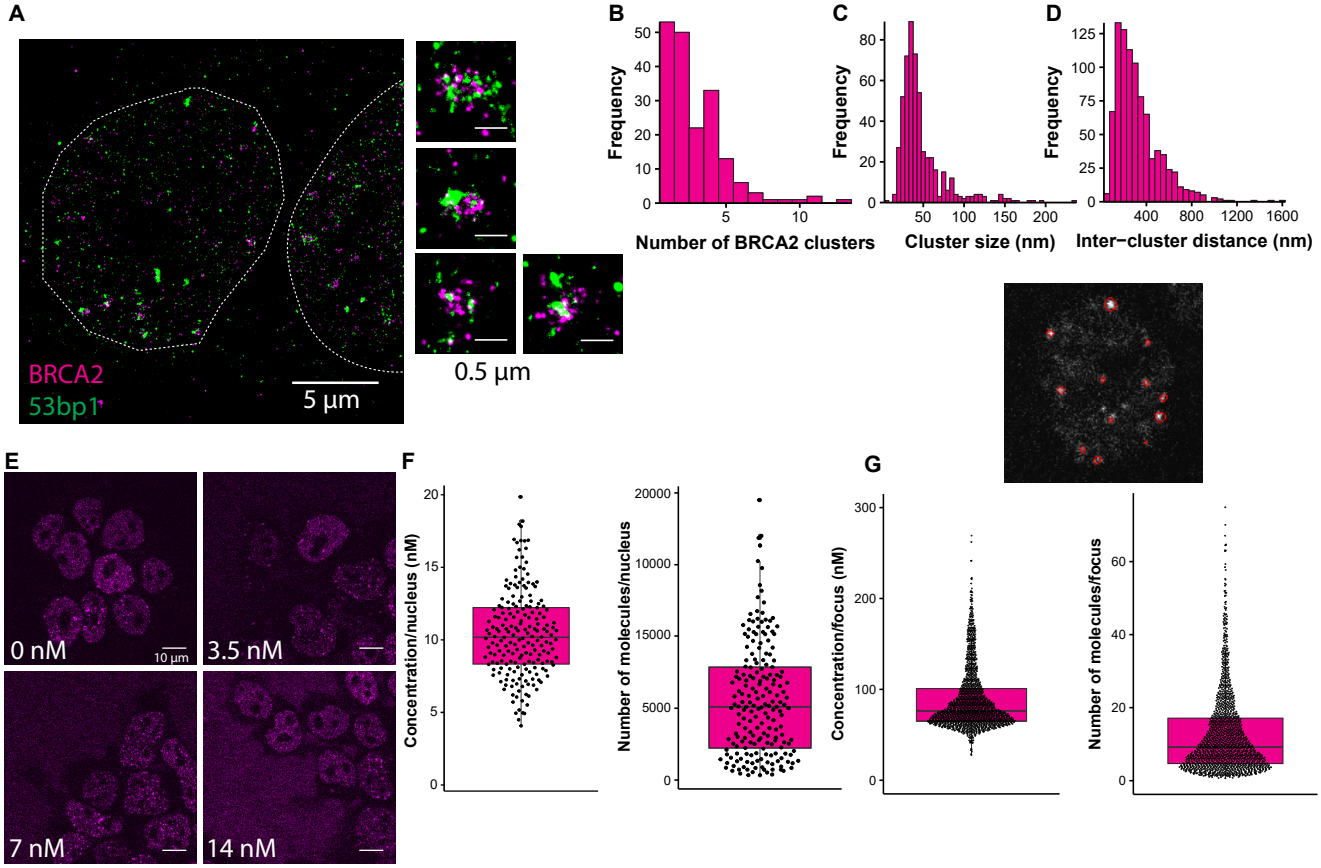

Figure 4. Nanoscale localization of BRCA2 in MMC-induced DNA repair foci and quantification of nuclear BRCA2 concentration. A Two-color dSTORM imaging of BRCA2-Halo::Alexa647 and 53bp1 (indirect immunofluorescence CF568). Typical examples of foci with both BRCA2 and 53bp1 signal. **B** Quantification of the number of BRCA2 clusters within individual automatically segmented 53bp1 foci. **C-D** Quantification of the size of the respective clusters and the center-to-center distance between the clusters within the individual foci. Data from 7 cells in total from two imaging sessions. **E** Cellular concentration of BRCA2 was estimated by titration of increasing concentrations of labeled GST-HaloTag protein in the cell medium. The voxel intensity was used to estimate the local concentration. **F** The nuclear concentration was estimated by 3D segmentation of the cell nuclei. The nuclear concentration is defined as the average nuclear concentration within all voxels in the 3D nuclear volume, whereas the number of BRCA2 molecules per nucleus is calculated by multiplying the concentration with the estimated nuclear volume. **G** Within the identified nuclei, the foci were segmented in 3D. The image shows an example of the segmentation in a single confocal slice. The plots show results from one replicate, results from additional replicates (n=3) are summarized in Figure S2

the local concentration and total number of BRCA2 molecules in individual nuclei. This shows a nuclear concentration of 10 nM or about 5,000 molecules per cell nucleus (Figure 4F). Additionally, we were able to segment individual BRCA2 foci to estimate the number of BRCA2 molecules per focus. This analysis indicates that the local concentration of BRCA2 is nearly 10 times higher within repair foci (100 nM) whereas the mean number of BRCA2 molecules per focus was estimated at approximately 25. The numbers we obtained are consistent with the analysis of the amount of BRCA2-Halo protein labeled with

JF646 and analyzed with SDS-Page) using a defined number of cells, while using labeled GST-HaloTag protein with defined concentration as a reference (S2). Quantification of the total intensity of the protein bands normalized to the amount of sample loaded reports the average number of BRCA2 molecules per nucleus. This method indicated that the number of molecules per cells is comparable to the numbers obtained by live cell imaging quantification.

Discussion

In this study we have investigated the dynamic behavior of BRCA2 specifically at 53bp1 foci induced by the DNA crosslinker mitomycin C. Instantaneous multiplane two-color imaging allowed us to detect the BRCA2 molecules located in DNA repair foci and study their mobility. Previous single-molecule tracking studies of BRCA2 have shown an increase of the immobile fraction of BRCA2 after DNA damage induction (8, 12). Here, we show that this immobilization is caused by BRCA2 localized to DNA repair foci. We identified that only about 20% of the BRCA2 molecules that were tracked inside the nucleus were accumulated at the foci, which explains the subtle increase in immobilization of BRCA2 measured in the entire nucleus, as we previously observed. In depth-analysis of the 3D tracking data revealed that next to the increased immobilization, diffusing BRCA2 molecules inside the foci show an increase in confined mobility. This confined motion is most evident in slow moving BRCA2 molecules, with an increased confinement for molecules displacing between 80 and 150 nm. A similar pattern of confined motion is observed for BRCA2 molecules outside foci, but to a lesser extent (Figure 3F). Similar confined motion patterns have been observed for other nuclear proteins such as CTCF and transcription factors (Sox2 and Oct4) (6, 7, 22), contributing to the function of these proteins, such as improved target search in chromatin. In case of the BRCA2 complexes this could be a mechanism to efficiently probe the chromatin environment for the presence of DNA damage. The difference in the chromatin environment (e.g. increase in histone modifications) present at DNA damage sites could enhance transient binding of BRCA2 complexes at the damaged chromatin. This will allow BRCA2, even at its low concentration, to dynamically associate with the damaged genomic region. This local difference in affinity could serve as a mechanism to retain and concentrate BRCA2 molecules at sites of DNA damage for a longer period and could explain the confined motion patterns we do observe for BRCA2. Consistently, we observed that transitions of BRCA2 from inside to outside a focus are reduced compared to a randomized situation, whereas molecules surrounding the focus have an increased probability to move into the focus.

A similar mechanism could operate within a focus. Our observation by single-molecule localization microscopy (Figure 4) of BRCA2 clusters within a focus suggests that the chromatin environment (e.g. distribution of histone modifications) within a focus is not homogeneous. The measured distance between these intra-focus BRCA2 clusters (Figure 4) is consistent with the possibility of displacement of BRCA2 molecules between these clusters (resulting in the class of BCRA2 molecules with confined motion), whereas molecules with larger displacements lose their association with the clusters. It remains to be investigated what interactions drive these confined motion patterns, but it should be considered that BRCA2 is present in complex with several other repair proteins such as PALB2 and RAD51. For example, loss of the PALB2-BRCA2 interaction prevents BRCA2 localization to foci (9). On the contrary, the accumulation of BRCA2 does not depend on its highly conserved DNA binding domain and C-terminal domain (8), which, at least in vitro, interact with (single-stranded) DNA (23). A possible explanation is that BRCA2 tethered to

chromatin surrounding the DNA damage through its N-terminal interaction with PALB2, without the requirement of all functional domains required to promote all BRCA2 functions. In this way the accumulation of BRCA2 is uncoupled from its canonical function of loading RAD51 at RPA coated DNA. It would be interesting in future studies to investigate how the confined mobility of BRCA2 changes over time during the repair process.

Mechanisms of accumulation of repair factors at DNA lesions

The dynamics of several different DNA repair proteins has been investigated in living cells. It shows that although many of these proteins accumulate at sites of DNA damage, they can do so through different mechanisms (24). Whereas RAD51 and RPA are stably bound (14, 25), RAD54, another protein in the same DNA repair pathway, shows a very dynamic behavior (14). Interestingly, while RAD54 visually accumulates in foci, immobilization of the protein is hardly observed, unless its ATP activity is affected (26). In recent years liquid-liquid phase separation (LLPS) has been proposed as a mechanism to drive compartmentalization of proteins in DNA repair foci, as well as in many other nuclear and cellular processes. 53bp1 is one of the DNA repair factors that forms accumulations with liquid-like characteristics (27, 28). Additionally, RAD52 (functional homolog of BRCA2 in yeast) can form condensates in vitro and in vivo (29). A different study using single-molecule tracking showed that RAD52 in budding yeast shows reduced mobility at foci (25). However, compared to the RPA subunit Rfa1, which shows clear immobilization, the diffusion of RAD52 is only reduced. For the formation of condensates proteins need to be present at a high enough concentration, however BRCA2 is present at a low concentration in the cell nucleus and within the foci only tens of BRCA2 molecules are present. This suggests that BRCA2 by itself is not phase separated, but rather is trapped in DNA lesion-containing compartments where it undergoes transient immobilization through interaction with other proteins in the foci. This causes it to reside at the foci longer, resulting in an increased concentration. This might give BRCA2 enough time to exert its function. A recent study indicates that throughout the lifetime of a 53bp1 focus, the phase of the foci transitions from a liquid to solid-like state. The local chemical environment at the damaged site could therefore act as a crucial mechanism to regulate the outcome of the repair, to which proteins such as BRCA2 could respond. Compared to RAD52, which in foci shows slower diffusion, but no immobilization, BRCA2 shows increased immobilization, but also confined diffusion. However, no change in diffusion rate is observed for diffusing molecules of BRCA2. Possibly, proteins such as 53bp1 and RAD52, which are much more abundant in the cell, can form phase-separated compartments and then mediate the accumulation of other factors such as BRCA2 at DNA lesions.

Dynamic organization of BRCA2 at DNA repair foci

In line with our previous publication on the localization of BRCA2 using antibodies, BRCA2-HaloTag localizes in small clusters at the DNA break sites in fixed cells. Quantification of the amount of BRCA2 in cell nuclei and repair foci specifically shows that only tens of BRCA2 molecules are present in DNA repair foci; therefore, individual clusters of BRCA2 within a focus will contain only a few BRCA2 molecules (Figure 4). The emerging picture from several studies that use superresolution microscopy to study the architecture of DNA repair foci is that proteins organized in repair foci in specific patterns rather than a homogeneous mix of different repair factors (30–32). For example, we have observed by single-molecule localization microscopy that part of the RAD51 proteins that are present at repair foci do not localize with BRCA2 (21). It is interesting to consider that even for proteins that are suggested to accumulate by LLPS, such as 53bp1, there is still spatial inhomogeneity of the protein within the focus, instead of a homogeneous distribution of

protein. A challenge for future studies will be to converge the observed mobility patterns of the different proteins with their nanoscale localization at foci. An important aspect that still needs to be addressed is how dynamic the overall organization of repair foci is. Future studies using super-resolution microscopy in living cells, possibly combined with machine learning to enhance spatial and temporal resolution, will hopefully allow to further delineate the significance of spatiotemporal dynamics of DNA repair foci that protect the cells against genomic instability.

Material and Methods

Cell culture

Mouse ES cells were maintained on 0.1% gelatin (Sigma) coated plates in mouse ES cell medium (DMEM, 40% BRL-conditioned medium, 10% FCS (Capricorn Scientific), supplemented with pen-strep, non-essential amino acids (Lonza) and leukaemia inhibitory factor (1000 U/ml) and 0.1 mM β-mercapto-ethanol). For ac-MFM experiments, cells were kept for a few passages prior to the experiments in DMEM Knockout medium (Thermofisher) supplemented with 10% FCS (Sigma, F2442), pen-strep, LIF, NEAA and 0.1 β-mercapto-ethanol.

DNA constructs

The EGFP-tr53bp1 construct was assembled using Gibson Assembly with a fragment of human 53bp1 (amino acids 1221-1709, Addgene #69531) (19) that was cloned in a EGFP Piggybac vector (33).

Cell lines

The BRCA2-HaloTag knock-in mouse embryonic stem cell line that is used in this paper is as described in Paul et. al (2021). EGFP-53bp1trunc Piggybac vector was transfected in BRCA2-HaloTag cells together with CMV-Hypbase piggybac transpose plasmid using Lipofectamine 3000 according to manufacturer's protocol. Cells were selected with puromycin for 1 week after which the selected population was used for the experiments.

Sample preparation of live cell imaging

Between 20,000 and 40,000 cells were seeded the day before the imaging experiment on 8-well ibidi dishes coated with 25 µg/ml laminin (Roche, 11243217001). When indicated cells were treated with 1 µg/ml mitomycin C (Sigma, M0503). For HaloTag labelling, medium was replaced and subsequently cells were labelled with 50 nM JF549-HaloTag dye, unless a different concentration is indicated, followed by washing with PBS and replacement with fresh medium. Imaging was done in FluoroBrite DMEM medium (ThermoFisher, A1896701) complemented with 10% FCS, pen-strep, LIF, NEAA, 0.1 mM β-mercapto-ethanol.

Sample preparation for immunofluorescence

The cells were grown in 8-well glass bottom dishes (Ibidi) or round coverslips (#1.5H), coated with laminin as described above. For fixation cells were washed with PBS once and fixed with 4% PFA (Thermo-Fisher) in PBS for 10 minutes. Cells were washed with PBS with 0.1% triton for 3 times followed by 2 times 10 minutes washing steps. Cells were blocked with 3% BSA in PBS for 20 minutes followed by incubation of the primary antibodies in blocking buffer. After washing with PBS with 0.1% Triton cells were incubated with fluorescently labelled secondary antibodies for 1 hour at room temperature. For immunostaining of 53bp1 a rabbit polyclonal antibody was used (1:1000, Novus biologicals, NB100-304) together with anti-rabbit F(ab')2 fragment conjugated with CF568 (1:1000,

Sigma, SAB4600310). For dSTORM imaging of HaloTag proteins, cells were incubated with 500 nM AF647-HaloTag ligand (kind gift from Luke Lavis) together with the primary antibodies in blocking buffer for 2 hours at room temperature.

Ac-MFM setup

The ac-MFM system was as described in Abrahamson et al. (16). In brief, specimens are imaged on a Nikon TiE epi-fluorescence microscope with a 100x 1.45NA Plan Apo objective lens (Nikon), and illuminated by 3-6kW/cm2 561nm laser excitation. Fluorescence was collected and passed through a custom multi-focal grating and color correction grating as described by Abrahamsson et al. Nine focal planes are imaged onto a EMCCD detector (iXon DU897, Andor) up to 30 Hz. The focal position of the microscope was maintained by active stabilization. Every day, prior to the imaging experiments a sample with mounted 100 nm Tetraspeck beads (ThermoFisher) was used to correct for chromatic aberrations, measure the z-slice separation distance, determine relative z-plane detection efficiency, and to align image channels. A Tokai Hit microscope stage holder was used to maintain cells at 37C with 5% CO2. Movies of 2000 frames were recorded, where every 50th frame the GFP signal was also recorded. Sample was illuminated continuously with 561nm light and low 405 nm light for photoactivation of Halo-JF549.

Confocal imaging and FRAP

Confocal and FRAP experiments were done on a Zeiss Elyra PS1 system with a Tokai Hit stage incubator calibrated on 37 ºC and 5% CO2. 63x objective (NA 1.4 Plan Apo). For both FRAP experiments (Figure 1) and quantitative confocal experiments (Figure 4) a GaAsP detector was used. FRAP experiments were acquired using a square ROI of 1.14x1.14 µm, which was scanned at 0.2s interval, with 20 frames pre-bleach, 4 frames bleaching at full laser power, followed by 230 frames to record recovery. Cells that moved too much during the acquisition were excluded from the analysis. Mean intensity from the bleach ROI was measured over time. The intensity traces were normalized by the mean intensity of frame 10-20 before bleaching. The figure shows the average normalized intensity trace of multiple experiments, whereas the shading represents the SEM of the intensity (standard deviation/sqrt(N cells)).

dSTORM

Imaging was performed using a Zeiss Elyra PS1 system using a 100x 1.46NA Korr α Plan Apochromat objective. 561 and 642 100mW diode lasers were used to excite the fluorophores together with respectively a BP 570–650 + LP 750 or LP 655 excitation filter. dSTORM imaging was done using near-TIRF (HiLo) settings while the images were recorded on Andor iXon DU 897, 512x512 pixel EMCCD camera.
For drift correction and channel alignment 100 nm Tetraspeck beads (ThermoFisher) were added to the sample. To perform dSTORM imaging, an imaging buffer was prepared containing 40mM MEA (Sigma), 0.5mg/ml Glucose Oxidase (Sigma), 40 µg/ml Catalase (Sigma) and 10% w/v Glucose in Tris pH 8.0. The dSTORM images were acquired sequentially, starting with the Alexa 647 staining followed by imaging CF568. At least 10 000 images were acquired at an interval of 33ms per frame. The raw data was analyzed by ZEN software. Molecules were localized and a drift correction was applied using image correlation in the two images separately. Subsequently the two images were combined and the channels were aligned laterally using 100nm Tetraspeck beads that are deposited into the sample.

Image analysis for ac-MFM

Raw images from ac-MFM microscope were converted to 3D stacks and corrected for

chromatic aberrations in MATLAB (https://github.com/aicjanelia/MFM) and processed using background subtraction and Richardson-Lucy deconvolution (7px rolling ball, 5 iterations, respectively). Subsequently, molecules were localized and tracked in 3D using Mosaic plugin (34) in ImageJ after pre-processing using and Gaussian blur denoising (0.7px radius). A fixed intensity threshold of 800 a.u. was set. Molecules were linked at a maximum frame-to-frame distance of 500 nm. EGFP-tr53bp1 movies, that were used to define the DNA damages sites, were processed in Matlab, where frames were identified that contained EGFP signal, the signal in intermediate frames was interpolated linearly based on the image frame before and after. The foci signal was identified using difference of Gaussian edge detection and a binary mask was created. Next for every point of the tracks it was determined whether it was in or outside the mask. To compare the results to a random situation, data sets were generated by randomly redistributing the identified 3D objects at the first frame of the movie, along x-y axes in the image plane within the convex hull surrounding the centers of mass of all foci. MATLAB routines used for the analysis can be found on https://github.com/maartenpaul/MFManalysis_Matlab/ (based on original code repositories: https://github.com/aicjanelia/MFM and https://gitlab.com/aicjanelia/visitor-maarten-paul)
Subsequently a script in R was used for further processing of the tracks and plotting of the data (https://github.com/maartenpaul/MSDanalysis_MFM). Python code to segment the tracks into different mobile states using deep learning and to estimate the mean-square-displacement and moment scaling spectrum of the individual tracklets (20) was incorporated in Rstudio using the reticulate package (35). For further analysis track(lets) that were present at least one frame in their lifetime inside the mask were considered associated with the DNA damage. The angle (α) between displacements within the track(lets) was calculated in 2D as described in Hansen (2019) (7). For the angle analysis displacements immobile tracklets and x-y displacements below 100nm were excluded from the analysis.

Image analysis dSTORM

For quantification of BRCA2 clusters, 53bp1 foci were identified by applying an Otsu threshold on the 53bp1 images and saved as ImageJ ROIs. The ROIs were imported in R and BRCA2 localizations that are within the ROIs were clustered using Voronoi tessellation (36). After conversion of the localizations to a Delaunay diagram, the length of all vertices was calculated. All vertices longer than 30 nm were removed and isolated clusters of linked localizations were identified. To remove spare localizations, clusters with less than 5 localizations were filtered out. Shape features describing these clusters were determined using the SMoLR package (37). The size of clusters is defined as mean of the FWHM of the major and the minor axis of the localizations within the cluster. The distance of the clusters is determined as the distance between centre-of-mass of the two cluster within the same segmented 53bp1 focus.

Quantification of cellular concentration of BRCA2

HaloTag-GST (61 kDa) (Promega, G4491) was labeled with JF646 for 4 hours at 4° C on ice with 3x excess HaloTag ligand (buffer: 1x PBS, 20% glycerol, 1 mM DTT). Followed by removal of the unreacted HaloTag ligand using a Zeba desalting column (7K MWCO, 0.5 ml, ThermoFisher, 89882). Using SDS-PAGE it was confirmed that the protein was recovered after labeling and elution from the column. The concentration of the labelled protein was validated using Nanodrop and on SDS-Page using a BSA with known concentration. Subsequently this labelled protein was used as reference to estimate the amount of BRCA2 per cell. The nuclei of live cells were segmented in 3D using a routine in Track-

mate (38), which makes use of Stardist (39) for 2D segmentation of nuclei, followed by connecting the matching nucleus segmentation in the 3D image stack. A 3D label image was exported and used in a custom-made routine in CellProfiler (40). The label image was used to generate 3D nuclei objects and was used to determine the nuclear volume and the integrated intensity of the BRCA2-Halotag intensity. BRCA2 foci were segmented using an adaptive threshold in 3D and the volume and intensity were measured. The CellProfiler pipeline and accompanying R code for processing and plotting the data is available at https://github.com/maartenpaul/Halo_cell_quant. The integrated intensity (a.u.) was converted to concentration and number of molecules by comparing the intensity to a titration curve of the labeled HaloTag- GST::JF646 standard protein. Using this titration curve, the intensity per pixel can be converted to the local concentration of HaloTag protein. Assuming that the segmented nuclei are much larger than the confocal volume per pixel, this conversion can be used to estimate the concentration of BRCA2 in the nuclei. The concentration can subsequently converted to number of molecules per nucleus by dividing over the volume and Avogadro's number. The results were compared with an in-gel analysis of in vivo labelled BRCA2-HaloTag. BRCA2 was labelled with JF646 HaloTag ligand in living cells grown on plates. Subsequently, cells were trypsinized and the cell concentration was determined. Cells were resuspended at 25,000 cell/µl and treated with benzonase in buffer with protease inhibitors (2 mM MgCl2, 20 mM Tris pH 8, 10% glycerol, 1% triton X-100 and 25 U/ml benzonase) and subsequently lysed by adding 2x Laemmli buffer at equal volume. Cell lysates were run on 3-8% SDS-Page Tris-Acetate gel. The fluorescently labelled proteins were imaged in the gel using a Typhoon gel imager (Amersham).

Data availability

Software code used for the analysis of the data is available on Github in the repositories indicated in the Materials and Methods sections. The processed data is available at Zenodo (doi: https://doi.org/10.5281/zenodo.7516461), whereas raw data is kindly provided on request due to the large size of the data sets.

ACKNOWLEDGEMENTS

The authors would like to dedicate this work to our friend and colleague Claire Wyman, who passed away during completion of this research. Aberration-corrected multifocal microscopy (acMFM) was performed in collaboration with the Advanced Imaging Center at Janelia Research Campus, a facility jointly supported by the Gordon and Betty Moore Foundation and the Howard Hughes Medical Institute. The experimental visit to Janelia was supported by a Journal Cell Science travel grant. This study was supported by the Oncode Institute, which is partly financed by the Dutch Cancer Society. We thank the Josephine Nefkens Cancer Program for infrastructure support. We thank the Optical Imaging Centre at the Erasmus MC for use and technical assistance with the Zeiss Elyra microscope. We thank Luke Lavis (HHMI Janelia) for providing HaloTag ligands and Maayke Kuijten for feedback on the manuscript and support in plasmid cloning.

AUTHOR CONTRIBUTIONS

MWP, JA, TLC, RK, and CW designed research; MWP and JA performed research; MWP, JA, EW, RvG and IS contributed new reagents/analytic tools; MWP, JA, EW, RvG, and IS analyzed data; MWP, RK and CW wrote the paper. All authors discussed the results and commented on the manuscript.

COMPETING FINANCIAL INTERESTS

All authors declare that they have no conflicts of interest.

Bibliography

1. A. Zelensky, R. Kanaar, and C. Wyman. Mediators of Homologous DNA Pairing. *Cold Spring Harbor Perspectives in Biology*, 6(12):a016451–a016451, December 2014. ISSN 1943-0264. doi: 10.1101/cshperspect.a016451.
2. Kimberly A. Rickman, Raymond J. Noonan, Francis P. Lach, Sunandini Sridhar, Anderson T. Wang, Avinash Abhyankar, Athena Huang, Michael Kelly, Arleen D. Auerbach, and Agata Smogorzewska. Distinct roles of BRCA2 in replication fork protection in response to hydroxyurea and DNA interstrand cross-links. *Genes & Development*, April 2020. ISSN 0890-9369, 1549-5477. doi: 10.1101/gad.336446.120.
3. Katharina Schlacher, Nicole Christ, Nicolas Siaud, Akinori Egashira, Hong Wu, and Maria Jasin. Double-Strand Break Repair-Independent Role for BRCA2 in Blocking Stalled Replication Fork Degradation by MRE11. *Cell*, 145(4):529–542, May 2011. ISSN 00928674. doi: 10.1016/j.cell.2011.03.041.
4. Richard Wooster, Graham Bignell, Jonathan Lancaster, Sally Swift, Sheila Seal, Jonathan Mangion, Nadine Collins, Simon Gregory, Curtis Gumbs, Gos Micklem, Rita Barfoot, Rifat Hamoudi, Sandeep Patel, Catherine Rices, Patrick Biggs, Yasmin Hashim, Amanda Smith, Frances Connor, Adalgeir Arason, Julius Gudmundsson, David Ficenec, David Kelsell, Deborah Ford, Patricia Tonin, D. Timothy Bishop, Nigel K. Spurr, Bruce A. J. Ponder, Rosalind Eeles, Julian Peto, Peter Devilee, Cees Cornelisse, Henry Lynch, Steven Narod, Gilbert Lenoir, Valdgardur Egilsson, Rosa Bjork Barkadottir, Douglas F. Easton, David R. Bentley, P. Andrew Futreal, Alan Ashworth, and Michael R. Stratton. Identification of the breast cancer susceptibility gene BRCA2. *Nature*, 378(6559):789–792, December 1995. ISSN 1476-4687. doi: 10.1038/378789a0.
5. Ignacio Izeddin, Vincent Récamier, Lana Bosanac, Ibrahim I Cissé, Lydia Boudarene, Claire Dugast-Darzacq, Florence Proux, Olivier Bénichou, Raphaël Voituriez, Olivier Bensaude, Maxime Dahan, and Xavier Darzacq. Single-molecule tracking in live cells reveals distinct target-search strategies of transcription factors in the nucleus. *eLife*, 3, June 2014. ISSN 2050-084X. doi: 10.7554/eLife.02230.
6. Zhe Liu, Wesley R Legant, Bi-Chang Chen, Li Li, Jonathan B Grimm, Luke D Lavis, Eric Betzig, and Robert Tjian. 3D imaging of Sox2 enhancer clusters in embryonic stem cells. *eLife*, 3, December 2014. ISSN 2050-084X. doi: 10.7554/eLife.04236.
7. Anders S. Hansen, Assaf Amitai, Claudia Cattoglio, Robert Tjian, and Xavier Darzacq. Guided nuclear exploration increases CTCF target search efficiency. *Nature Chemical Biology*, December 2019. ISSN 1552-4450, 1552-4469. doi: 10.1038/s41589-019-0422-3.
8. Maarten W Paul, Arshdeep Sidhu, Yongxin Liang, Sarah E van Rossum-Fikkert, Hanny Odijk, Alex N Zelensky, Roland Kanaar, and Claire Wyman. Role of BRCA2 DNA-binding and C-terminal domain on its mobility and conformation in DNA repair. *eLife*, 10:e67926, July 2021. ISSN 2050-084X. doi: 10.7554/eLife.67926.
9. Bing Xia, Qing Sheng, Koji Nakanishi, Akihiro Ohashi, Jianmin Wu, Nicole Christ, Xinggang Liu, Maria Jasin, Fergus J. Couch, and David M. Livingston. Control of BRCA2 Cellular and Clinical Functions by a Nuclear Partner, PALB2. *Molecular Cell*, 22(6):719–729, June 2006. ISSN 10972765. doi: 10.1016/j.molcel.2006.05.022.
10. Rimma Belotserkovskaya, Elisenda Raga Gil, Nicola Lawrence, Richard Butler, Gillian Clifford, Marcus D. Wilson, and Stephen P. Jackson. PALB2 chromatin recruitment restores homologous recombination in BRCA1-deficient cells depleted of 53BP1. *Nature Communications*, 11(1):1–11, February 2020. ISSN 2041-1723. doi: 10.1038/s41467-020-14563-y.
11. Jean-Yves Bleuyard, Marjorie Fournier, Ryuichiro Nakato, Anthony M. Couturier, Yuki Katou, Christine Ralf, Svenja S. Hester, Daniel Dominguez, Daniela Rhodes, Timothy C. Humphrey, Katsuhiko Shirahige, and Fumiko Esashi. MRG15-mediated tethering of PALB2 to unperturbed chromatin protects active genes from genotoxic stress. *Proceedings of the National Academy of Sciences*, 114(29):7671–7676, July 2017. ISSN 0027-8424, 1091-6490. doi: 10.1073/pnas.1620208114.
12. Marcel Reuter, Alex Zelensky, Ihor Smal, Erik Meijering, Wiggert A. van Cappellen, H. Martijn de Gruiter, Gijsbert J. van Belle, Martin E. van Royen, Adriaan B. Houtsmuller, Jeroen Essers, Roland Kanaar, and Claire Wyman. BRCA2 diffuses as oligomeric clusters with RAD51 and changes mobility after DNA damage in live cells. *The Journal of Cell Biology*, 207(5): 599–613, December 2014. ISSN 0021-9525, 1540-8140. doi: 10.1083/jcb.201405014.
13. Jesse Aaron, Eric Wait, Michael DeSantis, and Teng-Leong Chew. Practical Considerations in Particle and Object Tracking and Analysis. *Current Protocols in Cell Biology*, page e88, May 2019. ISSN 1934-2500, 1934-2616. doi: 10.1002/cpcb.88.
14. Jeroen Essers, Adriaan B. Houtsmuller, Lieneke van Veelen, Coen Paulusma, Alex L. Nigg, Albert Pastink, Wim Vermeulen, Jan H. J. Hoeijmakers, and Roland Kanaar. Nuclear dynamics of RAD52 group homologous recombination proteins in response to DNA damage. *The EMBO journal*, 21(8):2030–2037, April 2002. ISSN 0261-4189. doi: 10.1093/emboj/21.8.2030.
15. P. M. Krawczyk, T. Borovski, J. Stap, T. Cijsouw, R. t. Cate, J. P. Medema, R. Kanaar, N. A. P. Franken, and J. A. Aten. Chromatin mobility is increased at sites of DNA double-strand breaks. *Journal of Cell Science*, 125(9):2127–2133, May 2012. ISSN 0021-9533, 1477-9137. doi: 10.1242/jcs.089847.
16. Sara Abrahamsson, Jiji Chen, Bassam Hajj, Sjoerd Stallinga, Alexander Y Katsov, Jan Wisniewski, Gaku Mizuguchi, Pierre Soule, Florian Mueller, Claire Dugast Darzacq, Xavier Darzacq, Carl Wu, Cornelia I Bargmann, David A Agard, Maxime Dahan, and Mats G L Gustafsson. Fast multicolor 3D imaging using aberration-corrected multifocus microscopy. *Nature Methods*, 10(1):60–63, January 2013. ISSN 1548-7091, 1548-7105. doi: 10.1038/nmeth.2277.
17. Nadya Dimitrova, Yi-Chun M. Chen, David L. Spector, and Titia de Lange. 53BP1 promotes non-homologous end joining of telomeres by increasing chromatin mobility. *Nature*, 456(7221):524–528, November 2008. ISSN 1476-4687. doi: 10.1038/nature07433.

18. Francisca Lottersberger, Roos Anna Karssemeijer, Nadya Dimitrova, and Titia de Lange. 53BP1 and the LINC Complex Promote Microtubule-Dependent DSB Mobility and DNA Repair. *Cell*, 163(4):880–893, November 2015. ISSN 00928674. doi: 10.1016/j.cell.2015.09.057.
19. Katherine S. Yang, Rainer H. Kohler, Matthieu Landon, Randy Giedt, and Ralph Weissleder. Single cell resolution in vivo imaging of DNA damage following PARP inhibition. *Scientific Reports*, 5:10129, May 2015. ISSN 2045-2322. doi: 10.1038/srep10129.
20. Marloes Arts, Ihor Smal, Maarten W. Paul, Claire Wyman, and Erik Meijering. Particle Mobility Analysis Using Deep Learning and the Moment Scaling Spectrum. *Scientific Reports*, 9(1):1–10, November 2019. ISSN 2045-2322. doi: 10.1038/s41598-019-53663-8.
21. Humberto Sánchez, Maarten W. Paul, Małgorzata Grosbart, Sarah E. van Rossum-Fikkert, Joyce H. G. Lebbink, Roland Kanaar, Adriaan B. Houtsmuller, and Claire Wyman. Architectural plasticity of human BRCA2–RAD51 complexes in DNA break repair. *Nucleic Acids Research*, 45(8):4507–4518, May 2017. ISSN 0305-1048, 1362-4962. doi: 10.1093/nar/gkx084.
22. Jeffrey M Alexander, Juan Guan, Bingkun Li, Lenka Maliskova, Michael Song, Yin Shen, Bo Huang, Stavros Lomvardas, and Orion D Weiner. Live-cell imaging reveals enhancer-dependent Sox2 transcription in the absence of enhancer proximity. *eLife*, 8:e41769, May 2019. ISSN 2050-084X. doi: 10.7554/eLife.41769.
23. H. Yang. BRCA2 Function in DNA Binding and Recombination from a BRCA2-DSS1-ssDNA Structure. *Science*, 297(5588): 1837–1848, September 2002. ISSN 00368075, 10959203. doi: 10.1126/science.297.5588.1837.
24. Judith Miné-Hattab, Siyu Liu, and Angela Taddei. Repair Foci as Liquid Phase Separation: Evidence and Limitations. *Genes*, 13(10):1846, October 2022. ISSN 2073-4425. doi: 10.3390/genes13101846.
25. Judith Miné-Hattab, Mathias Heltberg, Marie Villemeur, Chloé Guedj, Thierry Mora, Aleksandra M Walczak, Maxime Dahan, and Angela Taddei. Single molecule microscopy reveals key physical features of repair foci in living cells. *eLife*, 10:e60577, February 2021. ISSN 2050-084X. doi: 10.7554/eLife.60577.
26. Sheba Agarwal, Wiggert A. van Cappellen, Aude Guénolé, Berina Eppink, Sam E.V. Linsen, Erik Meijering, Adriaan Houtsmuller, Roland Kanaar, and Jeroen Essers. ATP-dependent and independent functions of Rad54 in genome maintenance. *The Journal of Cell Biology*, 192(5):735–750, March 2011. ISSN 0021-9525, 1540-8140. doi: 10.1083/jcb.201011025.
27. Sinan Kilic, Aleksandra Lezaja, Marco Gatti, Eliana Bianco, Jone Michelena, Ralph Imhof, and Matthias Altmeyer. Phase separation of 53BP1 determines liquid-like behavior of DNA repair compartments. *The EMBO Journal*, 0(0):e101379, July 2019. ISSN 0261-4189. doi: 10.15252/embj.2018101379.
28. Fabio Pessina, Fabio Giavazzi, Yandong Yin, Ubaldo Gioia, Valerio Vitelli, Alessandro Galbiati, Sara Barozzi, Massimiliano Garre, Amanda Oldani, Andrew Flaus, Roberto Cerbino, Dario Parazzoli, Eli Rothenberg, and Fabrizio d'Adda di Fagagna. Functional transcription promoters at DNA double-strand breaks mediate RNA-driven phase separation of damage-response factors. *Nature Cell Biology*, 21(10):1286–1299, October 2019. ISSN 1476-4679. doi: 10.1038/s41556-019-0392-4.
29. Roxanne Oshidari, Richard Huang, Maryam Medghalchi, Elizabeth Y. W. Tse, Nasser Ashgriz, Hyun O. Lee, Haley Wyatt, and Karim Mekhail. DNA repair by Rad52 liquid droplets. *Nature Communications*, 11(1):1–8, February 2020. ISSN 2041-1723. doi: 10.1038/s41467-020-14546-z.
30. J. R. Chapman, A. J. Sossick, S. J. Boulton, and S. P. Jackson. BRCA1-associated exclusion of 53BP1 from DNA damage sites underlies temporal control of DNA repair. *Journal of Cell Science*, 125(15):3529–3534, August 2012. ISSN 0021-9533, 1477-9137. doi: 10.1242/jcs.105353.
31. Donna R. Whelan, Wei Ting C. Lee, Yandong Yin, Dylan M. Ofri, Keria Bermudez-Hernandez, Sarah Keegan, David Fenyo, and Eli Rothenberg. Spatiotemporal dynamics of homologous recombination repair at single collapsed replication forks. *Nature Communications*, 9(1):3882, September 2018. ISSN 2041-1723. doi: 10.1038/s41467-018-06435-3.
32. Fena Ochs, Gopal Karemore, Ezequiel Miron, Jill Brown, Hana Sedlackova, Maj-Britt Rask, Marko Lampe, Veronica Buckle, Lothar Schermelleh, Jiri Lukas, and Claudia Lukas. Stabilization of chromatin topology safeguards genome integrity. *Nature*, 574(7779):571–574, October 2019. ISSN 1476-4687. doi: 10.1038/s41586-019-1659-4.
33. Alex N. Zelensky, Joost Schimmel, Hanneke Kool, Roland Kanaar, and Marcel Tijsterman. Inactivation of Pol θ and C-NHEJ eliminates off-target integration of exogenous DNA. *Nature Communications*, 8(1), December 2017. ISSN 2041-1723. doi: 10.1038/s41467-017-00124-3.
34. I. F. Sbalzarini and P. Koumoutsakos. Feature point tracking and trajectory analysis for video imaging in cell biology. *Journal of Structural Biology*, 151(2):182–195, August 2005. ISSN 1047-8477. doi: 10.1016/j.jsb.2005.06.002.
35. Kevin Ushey, J. J. Allaire, and Yuan Tang. Reticulate: Interface to 'Python', 2019.
36. Florian Levet, Guillaume Julien, Rémi Galland, Corey Butler, Anne Beghin, Anaël Chazeau, Philipp Hoess, Jonas Ries, Grégory Giannone, and Jean-Baptiste Sibarita. A tessellation-based colocalization analysis approach for single-molecule localization microscopy. *Nature Communications*, 10(1):1–12, May 2019. ISSN 2041-1723. doi: 10.1038/s41467-019-10007-4.
37. Maarten W. Paul, H. Martijn de Gruiter, Zhanmin Lin, Willy M. Baarends, Wiggert A. van Cappellen, Adriaan B. Houtsmuller, and Johan A. Slotman. SMoLR: Visualization and analysis of single-molecule localization microscopy data in R. *BMC Bioinformatics*, 20(1), December 2019. ISSN 1471-2105. doi: 10.1186/s12859-018-2578-3.
38. Dmitry Ershov, Minh-Son Phan, Joanna W. Pylvänäinen, Stéphane U. Rigaud, Laure Le Blanc, Arthur Charles-Orszag, James R. W. Conway, Romain F. Laine, Nathan H. Roy, Daria Bonazzi, Guillaume Duménil, Guillaume Jacquemet, and Jean-Yves Tinevez. TrackMate 7: Integrating state-of-the-art segmentation algorithms into tracking pipelines. *Nature Methods*, 19(7):

829–832, July 2022. ISSN 1548-7105. doi: 10.1038/s41592-022-01507-1.

39. Uwe Schmidt, Martin Weigert, Coleman Broaddus, and Gene Myers. Cell Detection with Star-convex Polygons. *arXiv:1806.03535 [cs]*, 11071:265–273, 2018. doi: 10.1007/978-3-030-00934-2_30.
40. Claire McQuin, Allen Goodman, Vasiliy Chernyshev, Lee Kamentsky, Beth A. Cimini, Kyle W. Karhohs, Minh Doan, Liya Ding, Susanne M. Rafelski, Derek Thirstrup, Winfried Wiegraebe, Shantanu Singh, Tim Becker, Juan C. Caicedo, and Anne E. Carpenter. CellProfiler 3.0: Next-generation image processing for biology. *PLOS Biology*, 16(7):e2005970, July 2018. ISSN 1545-7885. doi: 10.1371/journal.pbio.2005970.

Supplementary Figures

Supplementary movie 1: Example raw data single-molecule movie of BRCA2-Halo in a mitomycin C treated cells with 9 planes projected on the camera

Supplementary movie 2: Overlay of BRCA2-Halo single-molecule movie and interpolated EGFP-tr53bp1 mask in mitomycin C treated cell

Supplementary movie 3: Overlay of BRCA2-Halo single-molecule tracks and interpolated EGFP-tr53bp1 mask in mitomycin C treated cell

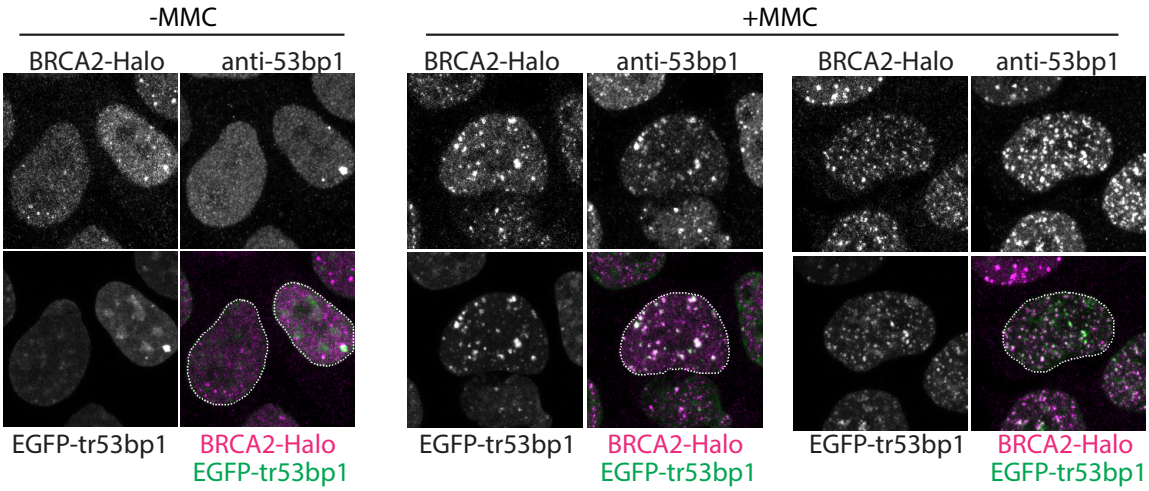

Figure S1. Validation of EGFP-tr53bp1 construct. Immunostaining against endogenous 53bp1 in fixed cells expressing BRCA2-HaloTag and EGFP-tr53bp1 without and with treatment with mitomycin C (MMC)

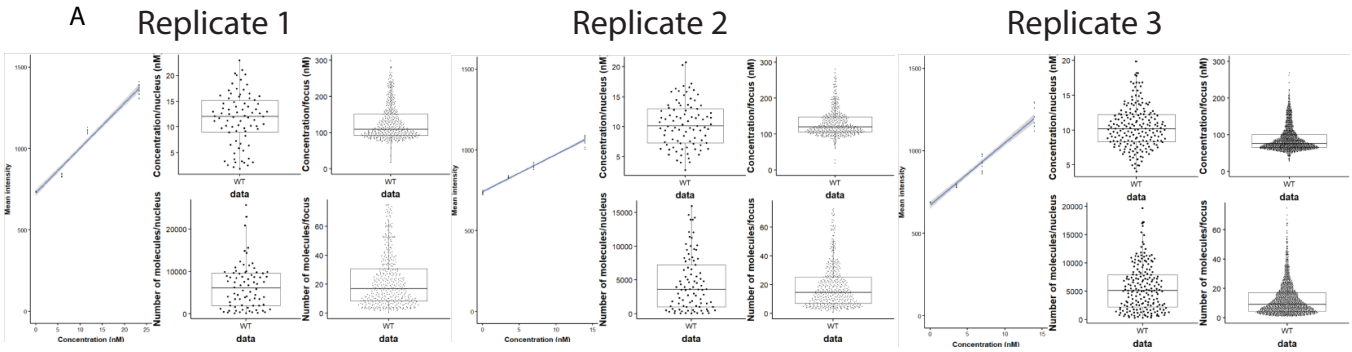

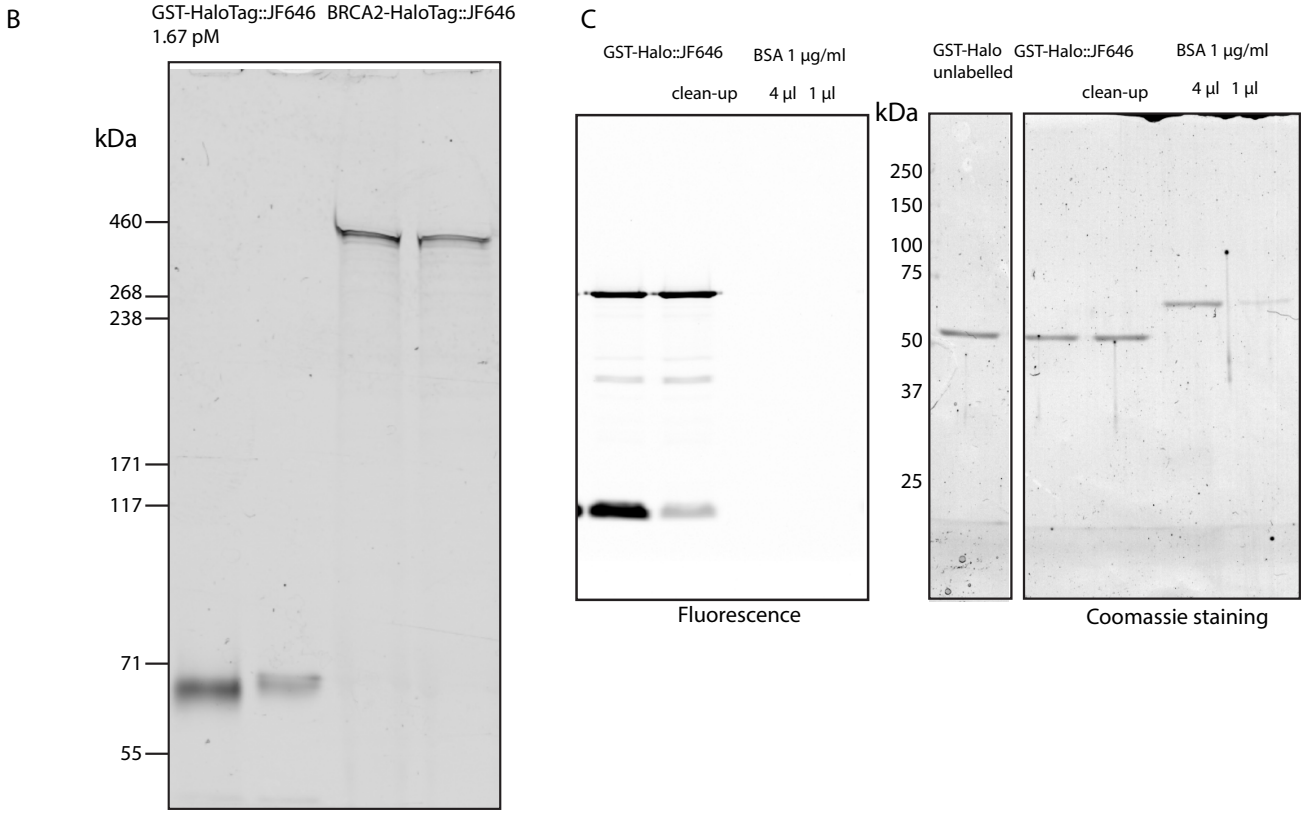

molecules/cell			500 000	200 000
volume (µl)	7.5	3	2194	1695
corrected a.u.	4505	1631	6.1	4.7
amount (fmol)	12.5	5.0	7350	5683

Figure S2. A Results of BRCA2-HaloTag quantification in knock-in cell lines treated with mitomycin C. Results of 3 replicates are shown of which the results of replicate 3 are shown in Figure 4. **B** Using a GST-HaloTag protein standard the number of molecules per cell and concentration was determined on a SDS page gel. C SDS-PAGE gel showing the results of labelling of the GST-HaloTag reference protein. Detected by fluorescence and by Coomassie staining to validate the concentration of the labeled protein.